First Measurement of the EMC Effect in ^{10}B and ^{11}B

A. Karki,[1] D. Biswas,[2] F. A. Gonzalez,[3] W. Henry,[4] C. Morean,[5] A. Nadeeshani,[2] A. Sun,[6] D. Abrams,[7] Z. Ahmed,[8] B. Aljawrneh,[9] S. Alsalmi,[10] R. Ambrose,[8] D. Androic,[11] W. Armstrong,[12] J. Arrington,[13] A. Asaturyan,[14] K. Assumin-Gyimah,[1] C. Ayerbe Gayoso,[15, 1] A. Bandari,[15] J. Barrow,[5] S. Basnet,[8] V. Berdnikov,[16] H. Bhatt,[1] D. Bhetuwal,[1] W. U. Boeglin,[17] P. Bosted,[15] E. Brash,[18] M. H. S. Bukhari,[19] H. Chen,[7] J. P. Chen,[4] M. Chen,[7] M. E. Christy,[2] S. Covrig,[4] K. Craycraft,[5] S. Danagoulian,[9] D. Day,[7] M. Diefenthaler,[4] M. Dlamini,[20] D. Dutta,[1] J. Dunne,[1] B. Duran,[12] C. Elliott,[5] R. Ent,[4] R. Evans,[8] H. Fenker,[4] N. Fomin,[5] E. Fuchey,[21] D. Gaskell,[4] T. N. Gautam,[2] J. O. Hansen,[4] F. Hauenstein,[22] A. V. Hernandez,[16] T. Horn,[16] G. M. Huber,[8] M. K. Jones,[4] S. Joosten,[23] M. L. Kabir,[1] C. Keppel,[4] A. Khanal,[17] P. M. King,[20] E. Kinney,[24] H. S. Ko,[25] M. Kohl,[2] N. Lashley-Colthirst,[2] S. Li,[26] W. B. Li,[15] A. H. Liyanage,[2] D. Mack,[4] S. Malace,[4] P. Markowitz,[17] J. Matter,[7] D. Meekins,[4] R. Michaels,[4] A. Mkrtchyan,[14] H. Mkrtchyan,[14] S.J. Nazeer,[2] S. Nanda,[1] G. Niculescu,[27] I. Niculescu,[27] D. Nguyen,[7] Nuruzzaman,[28] B. Pandey,[2] S. Park,[3] E. Pooser,[4] A. Puckett,[21] M. Rehfuss,[12] J. Reinhold,[17] N. Santiesteban,[26] B. Sawatzky,[4] G. R. Smith,[4] H. Szumila-Vance,[4] A. Tadepalli,[28] V. Tadevosyan,[14] R. Trotta,[16] S. A. Wood,[4] C. Yero,[17] and J. Zhang[3]

(for the Hall C Collaboration)

[1]*Mississippi State University, Mississippi State, Mississippi 39762, USA*
[2]*Hampton University, Hampton, Virginia 23669, USA*
[3]*Stony Brook University, Stony Brook, New York 11794, USA*
[4]*Thomas Jefferson National Accelerator Facility, Newport News, Virginia 23606, USA*
[5]*University of Tennessee, Knoxville, Tennessee 37996, USA*
[6]*Carnegie Mellon University, Pittsburgh, Pennsylvania 15213, USA*
[7]*University of Virginia, Charlottesville, Virginia 22903, USA*
[8]*University of Regina, Regina, Saskatchewan S4S 0A2, Canada*
[9]*North Carolina A & T State University, Greensboro, North Carolina 27411, USA*
[10]*Kent State University, Kent, Ohio 44240, USA*
[11]*University of Zagreb, Zagreb, Croatia*
[12]*Temple University, Philadelphia, Pennsylvania 19122, USA*
[13]*Lawrence Berkeley National Laboratory, Berkeley, California 94720, USA*
[14]*A.I. Alikhanyan National Science Laboratory*
(Yerevan Physics Institute), Yerevan 0036, Armenia
[15]*The College of William & Mary, Williamsburg, Virginia 23185, USA*
[16]*Catholic University of America, Washington, DC 20064, USA*
[17]*Florida International University, University Park, Florida 33199, USA*
[18]*Christopher Newport University, Newport News, Virginia 23606, USA*
[19]*Jazan University, Jazan 45142, Saudi Arabia*
[20]*Ohio University, Athens, Ohio 45701, USA*
[21]*University of Connecticut, Storrs, Connecticut 06269, USA*
[22]*Old Dominion University, Norfolk, Virginia 23529, USA*
[23]*Argonne National Laboratory, Lemont, Illinois 60439, USA*
[24]*University of Colorado Boulder, Boulder, Colorado 80309, USA*
[25]*Institut de Physique Nucleaire, Orsay, France*
[26]*University of New Hampshire, Durham, New Hampshire 03824, USA*
[27]*James Madison University, Harrisonburg, Virginia 22807, USA*
[28]*Rutgers University, New Brunswick, New Jersey 08854, USA*

(Dated: May 25, 2022)

The nuclear dependence of the inclusive inelastic electron scattering cross section (the EMC effect) has been measured for the first time in ^{10}B and ^{11}B. Previous measurements of the EMC effect in $A \leq 12$ nuclei showed an unexpected nuclear dependence; ^{10}B and ^{11}B were measured to explore the EMC effect in this region in more detail. Results are presented for ^{9}Be, ^{10}B, ^{11}B, and ^{12}C at an incident beam energy of 10.6 GeV. The EMC effect in the boron isotopes was found to be similar to that for ^{9}Be and ^{12}C, yielding almost no nuclear dependence in the EMC effect in the range $A = 4 - 12$. This is consistent with the earlier observation that the the EMC effect depends primarily on the local nuclear density due to the cluster structure of these nuclei.

PACS numbers: 13.60.Hb,25.30.Fj,24.85.+p

The modification of inelastic structure functions in nuclei (the EMC effect) is a clear indication that nucleons bound in a nucleus do not have the same quark structure as their unbound counterparts. Despite intense theoretical and experimental study since its first observation in 1983 [1], there is still no definitive explanation of the origin of the EMC effect [2, 3].

The observation that the EMC effect appears to scale with local (rather than average) nuclear density [4] instigated a paradigm shift in possible explanations of the EMC effect. It was subsequently found that the relative number of short-range correlated nucleon pairs (SRCs) in a nucleus (inferred from the ratio of the inclusive electron scattering cross section at $x > 1$ between nuclei and the deuteron) exhibited a similar density dependence [5]. Additional studies directly examined the correlation of the size of the EMC effect with SRCs [6, 7]. The high degree of correlation between these two nuclear effects reinforces the idea that the local nuclear environment plays an important role in the EMC effect. One explanation posits that the EMC effect is driven by changes in the nucleon structure due to local changes in nuclear density. It has also been suggested that the apparent connection between the EMC effect and SRCs can come about from highly virtual nucleons in a correlated pair, leading to large off-shell effects. Within the precision of existing data, both explanations have been found to be consistent with the observed correlation between the EMC effect and SRCs [7–9].

The local density (LD) and high virtuality (HV) hypotheses can be further explored by making additional measurements of the EMC effect and SRC ratios. Additional data on light nuclei will improve our understanding of the underlying nuclear physics driving both SRCs and the EMC effect. In addition, measurements at nearly-constant values of A covering a range in N/Z will help understand the impact of the isospin structure (since SRCs are dominated by n-p pairs [10–12]). Such measurements will be made at Jefferson Lab in experimental Hall C by experiments E12-10-008 (EMC) and E12-06-105 (SRC) [13, 14]. As part of the group of commissioning experiments that ran in Hall C after the completion of the Jefferson Lab 12 GeV Upgrade, a small subset of the planned EMC data were taken. We report on the results from this commissioning run, extracting the first measurement of the EMC effect in ^{10}B and ^{11}B. The Boron isotopes are of interest due to the fact that, like ^{9}Be, they are also expected to have significant α cluster contributions to their nuclear structure, while at the same time have an average density noticeably different from both ^{9}Be and ^{12}C. Measurement of the EMC effect in ^{10,11}B could provide additional confirmation that the α cluster configuration (and hence local nuclear density) plays a role or, alternately, indicate that ^{9}Be is an outlier for other reasons yet to be determined.

This experiment ran in parallel with JLab E12-10-002 (a measurement of inclusive electron scattering from hydrogen and deuterium) for about two days in February, 2018. The electron beam with energy 10.602±0.004 GeV impinged on 10 cm long LH2 and LD2 cryogenic targets and several solid targets; ^{9}Be, ^{12}C, ^{10}B$_4$C, and ^{11}B$_4$C. The B$_4$C targets were isotopically enriched to (at least) 95% by weight. The contribution from carbon to the B$_4$C yield was subtracted using measured yields from the carbon target.

Scattered electrons were detected in the new Super High Momentum Spectrometer (SHMS), a superconducting magnetic focusing spectrometer in a QQQD (three quadrupoles followed by a single dipole) configuration, with an additional small dipole (3° horizontal bend) just before the first quadrupole to allow access to small scattering angles. A detector package after the final dipole was used to identify electrons and provide tracking information for angle and momentum reconstruction. This detector package includes a pair of horizontal drift chambers, each chamber containing six planes of wires oriented at 0° and ±60° with respect to horizontal. The drift chambers provided position and direction information at the spectrometer focal plane; momentum and angle information at the target were reconstructed from this information via a fitted matrix transformation.

The detector hut also includes four hodoscope planes (three planes of scintillators and one quartz bar plane) for triggering and timing, as well as a gas Cherenkov (filled with 1 atm of CO$_2$) and a lead-glass calorimeter for electron identification. The detector package also includes another gas Cherenkov (typically filled with C$_4$F$_8$O at pressures below 1 atm) and an aerogel detector; these last two detectors were not used in this experiment. Additional measurements at the same central angle but over a reduced x range were also made in the High Momentum Spectrometer (HMS). Since the HMS was used extensively in the Jefferson Lab 6 GeV program, its performance and acceptance is more thoroughly understood than that of the SHMS and was used as a systematic check of the resulting target cross section ratios.

For the results presented in this work, measurements were made at a single SHMS central angle (21°) and three central momentum settings; $P_0 = 3.3$, 4.0, and 5.1 GeV. These spectrometer settings resulted in a coverage in Bjorken x of 0.3 to 0.95, while the four-momentum transfer, Q^2, varied from 4.3 to 8.3 GeV^2. The invariant mass of the hadronic system, W, is above the nominal nucleon resonance region ($W > 2$ GeV) up to $x \approx 0.7$.

Electron yields were binned in the fractional spectrometer momentum ($\Delta P/P$) and corrected for detector and tracking efficiencies as well as computer and electronic deadtimes. An additional correction was applied to the cryogenic targets for target density reduction due to beam heating. Backgrounds to the electron yields included pion contamination and contributions to the yield from charge symmetric processes. The latter were measured directly by flipping the spectrometer polarity and measuring the resulting positron yields. The positron yields scaled approximately with the radiation length of the target and were at most ≈1%. The pion contamination was determined by examination of the calorimeter spectra using segments of the default electron trigger less reliant on the calorimeter signal and was at most 0.5% at low x, but for values of x at which the pions were above threshold in the Noble Gas Cherenkov detector ($x = 0.58$), the pion contamination grew to be as large as 1.2%. For the cryotargets, contribution to the yield from the aluminum walls of the target cells was measured using two aluminum foils at the same positions along the beam as the ends of the cryotarget. The contribution to the yield was measured to be about 5% of the LD2 target yield with little variation as a function of x.

Yields were converted to cross sections via the Monte Carlo ratio method:

$$\left(\frac{d\sigma}{d\Omega dE'}\right)_{\mathrm{exp}} = \frac{Y_{\mathrm{exp}}}{Y_{\mathrm{sim}}}\left(\frac{d\sigma}{d\Omega dE'}\right)_{\mathrm{model}}, \qquad (1)$$

where Y_{exp} is the efficiency corrected, background subtracted experimental yield, Y_{sim} is the Monte Carlo yield produced using a model cross section, radiated using the Mo and Tsai formalism [17–19], and $\left(\frac{d\sigma}{d\Omega dE'}\right)_{\mathrm{model}}$ is the same model used to produce the simulated yield evaluated at Born level. Target cross section ratios were formed for each $(\Delta P/P)$ bin, converted to x, and grouped in bins of fixed width in x, $(\Delta x = 0.025)$.

So-called isoscaler corrections were applied to ^{9}Be and ^{11}B to account for the difference between the inelastic neutron and proton cross sections, σ_n and σ_p:

$$\left(\frac{\sigma_A}{\sigma_D}\right)_{\mathrm{ISO}} = \frac{\frac{A}{2}(\sigma_p+\sigma_n)}{(Z\sigma_p+N\sigma_n)}\frac{\sigma_A}{\sigma_D} = \frac{\frac{A}{2}(1+\frac{\sigma_n}{\sigma_p})}{(Z+N\frac{\sigma_n}{\sigma_p})}\frac{\sigma_A}{\sigma_D}, \qquad (2)$$

where A and Z are the usual atomic weight and atomic number, with $N = A - Z$, and σ_A/σ_D is the cross section ratio per nucleon. As described in Ref. [15], we use the effective cross sections for nucleons bound in the deuteron [20] to evaluate σ_n/σ_p. A correction is also applied to account for acceleration (deceleration) of the incoming (outgoing) electrons in the Coulomb field of the nucleus. This correction is calculated using a modified version of the Effective Momentum Approximation (EMA) [4, 21] and in the DIS region ranges from 0.16% at $x = 0.3$ to 0.5% at $x = 0.7$ for carbon (smaller for lighter nuclei). At larger values of x, the correction grows to ≈0.8% at $x = 0.95$.

We divided the systematic uncertainty in the EMC cross section ratios into three categories: point-to-point, x-correlated, and normalization uncertainties. Note that some quantities can contribute to more than one kind of uncertainty.

- Point-to-point uncertainties are assumed to be independent for each target and x-bin and contribute to the uncertainty in a manner similar to the statistical uncertainty. The largest of these uncertainties include those assigned to account for variation in the beam current/charge calibration over time (0.34%), variations across the spectrometer momentum bite in the extended target acceptance as compared to the thin, solid targets (0.5%), and kinematic dependent contributions to the radiative corrections (0.5%). Other, smaller contributions included those from electronic dead time, detector efficiency, and target density reduction. The total point-to-point uncertainty in the EMC ratios was estimated to be 0.87%

- So-called x-correlated uncertainties vary in size with x, but impact all points simultaneously. These include uncertainties due primarily to kinematic quantities, like beam energy, scattering angle, and spectrometer central momentum. In the region x=0.3-0.7, these uncertainties are on the order of 0.1%, but can grow to 1.22% at the very largest values of x.

- Normalization uncertainties contribute to the all points collectively, affecting the overall scale of the ratio. Significant sources of normalization uncertainty include the LD2 target thickness (0.6%), solid target thicknesses (0.5-0.66%), target wall subtraction (0.5%), and a contribution to the radiative correction uncertainty due to the difference in target radiation lengths and input cross-section models (0.5%). An additional 0.5% normalization uncertainty was assigned to account for possible acceptance issues hypothesized to explain the difference in EMC ratios observed between the SHMS and HMS. A renormalization factor (to be discussed below) was also applied, and we apply a 1% uncertainty due to this correction. The total normalization uncertainty was 1.58%-1.63%.

Upon initial extraction of the EMC ratios, it was found that the results were systematically smaller than previous measurements by about 2%. Subsequent investigation found no issues with the data analysis that would impact the ratio. Cross-checks with data taken in the HMS over a more limited x range showed some disagreement (at the 0.5% level) with the SHMS, suggesting there were possible effects due to differing acceptance for long 10 cm targets and the shorter targets, but not large enough to explain the whole discrepancy. Since the normalization issue exists for all four EMC ratios, we hypothesize that there is an unknown effect with respect to the deuterium target thickness or density, and fit a normalization correction to the ratios by fitting a single factor to all four targets making use of the empirical observation that the EMC effect is 1.0 at $x = 0.3$, independent of target. The extracted normalization factor is 1.020 and is applied to

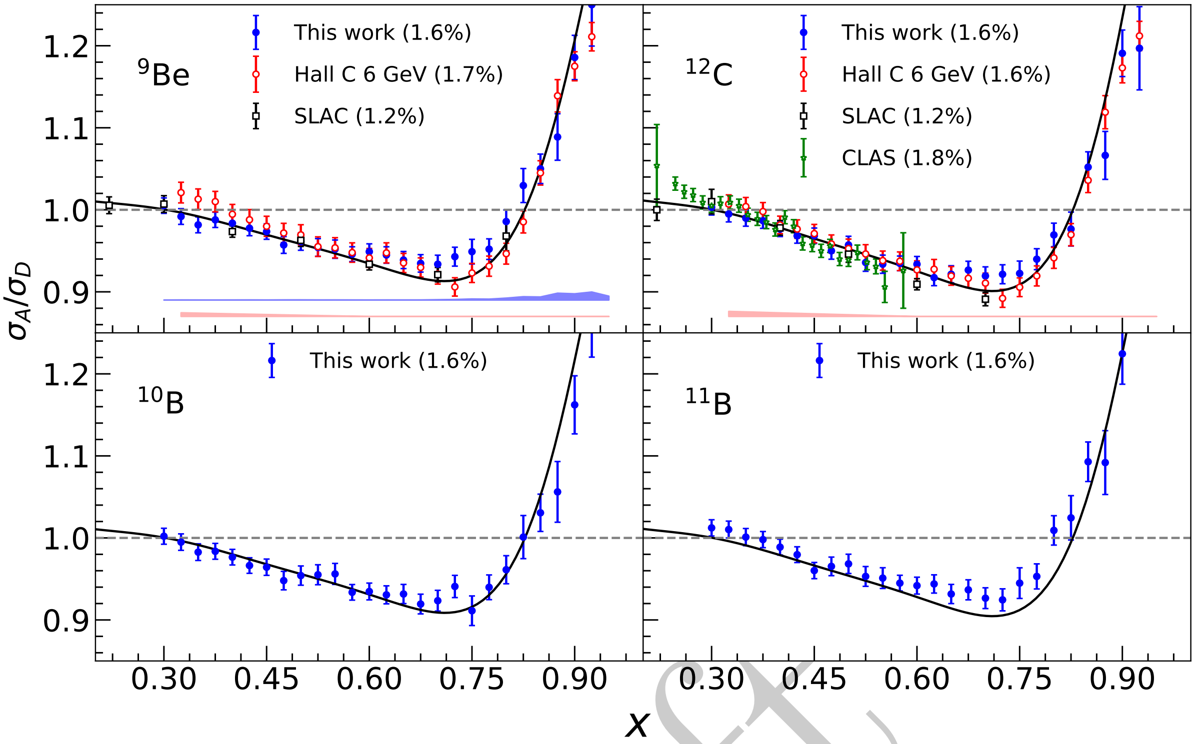

FIG. 1. Ratio of cross section per nucleon vs. x, for ^{9}Be, ^{10}B, ^{11}B, and ^{12}C from this experiment (blue, closed circles). The ^{9}Be and ^{12}C plots include the final results from JLab Hall C at 6 GeV [15] (open red circles) as well as those from SLAC E139 [16] (open black squares). Also shown are the carbon results from JLab CLAS at 6 GeV [8] (green stars). Error bars include statistics combined with point-to-point systematic errors and the normalization error for each experiment is noted in the label. The red band denotes the x-correlated error for the JLab Hall C 6 GeV results, while the blue band shows the x-correlated error for this experiment (only shown for beryllium since it is largely target independent). The solid black curve is the A-dependent fit of the EMC effect from SLAC E139 [16].

all the results shown here. Since the source of the normalization issue remains unknown, and the observation that the EMC effect be 1.0 at $x = 0.3$ is limited by the precision of previous world data, we assign an additional 1% uncertainty to the normalization due to this correction. In subsequent discussion, we will examine the slope of the EMC ratio between $0.3 < x < 0.7$ as a primary measurement of the size of the EMC effect. The slope has only small sensitivity to the overall normalization of the EMC ratio, so the normalization factor and its uncertainty have little impact on our main results.

The EMC ratios as a function of x for all four nuclei measured in this experiment (^{9}Be, ^{11}B, and ^{10}B, ^{12}C) are shown in Figure 1. Our results for ^{9}Be and ^{12}C are plotted along with the those from the JLab Hall C 6 GeV experiment [4] and SLAC E139 [16]. Results from the CLAS spectrometer in Hall B at 6 GeV [8] are also shown for carbon. In general, there is good agreement between data sets for ^{9}Be and ^{12}C with respect to the x dependence of the ratio. The ratios for ^{10}B and ^{11}B are the first measurement of the EMC effect for these nuclei.

The size of the EMC effect can be more precisely described using the magnitude of the slope, $|dR_{\mathrm{EMC}}/dx|$ in the region $0.3 < x < 0.7$ (the "EMC region"). These slopes are shown in Figure 2 (top), where the magnitude of the EMC effect is plotted vs. the scaled nuclear density. The scaled nuclear density is calculated from Green's Function Monte Carlo calculations of the nucleon spatial distributions [22] with an additional correction applied to account for the finite size of the nucleon. In addition, the density is scaled by $(A-1)/A$ to account for the fact that we are interested in the density of the $A-1$ nucleons seen by the struck nucleon. Note that the densities presented here are slightly different from those in Ref. [4] due primarily to updated distributions for carbon, resulting most visibly in a change in the relative density as compared to ^{4}He (previously, the resulting density for carbon was larger than that for ^{4}He). The EMC slopes from this experiment include an additional systematic uncertainty of 0.009 (≈ 4.5% of the slope) from the variation in the range of x over which the slope was extracted.

Fig. 2 (top) also includes slopes from the results from all experiments included in Fig. 1. Grey bands denote the combination of all experiments for a given target, where appropriate. With the higher precision provided by this determination of the size of the EMC effect, some

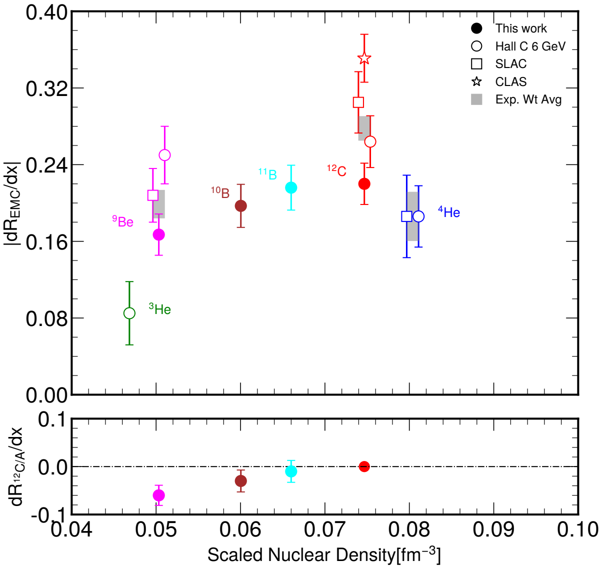

FIG. 2. Top: Size of the EMC effect (slope from the cross section ratio for $0.3 < x < 0.7$) vs. scaled nuclear density ($\rho(A-1)/A$) for ^{3}He, ^{4}He, ^{9}Be, ^{10,11}B, and ^{12}C. Closed circles are from this work, open circles from the JLab, Hall C 6 GeV results [15], open square from SLAC E139 [16], and open star from CLAS at 6 GeV [8]. Some points have been offset horizontally for visibility. Grey bands denote the weighted average of all experiments shown for a given target (where applicable). Bottom: Slope extracted from the cross section ratios of ^{12}C to ^{9}Be, ^{10}B, and ^{11}B from this experiment.

tension between the data sets is apparent. For ^{9}Be, the 6 GeV Hall C data and the results from this work are both in agreement with the SLAC E139 results, but are in slight disagreement with each other. This could be due to systematic effects in the radiative corrections,which are significantly larger for the 6 GeV data. On the other hand, the 6 GeV Hall C results agree with those from this experiment for carbon, although the latter are in some tension with the SLAC E139 and CLAS ratios. It is worth noting that the EMC ratios from the CLAS experiment for all targets appear to be systematically larger than those from other experiments as shown in Ref. [15].

We can more precisely compare the size of the EMC effect in ^{12}C to the other targets studied in this experiment by taking the direct cross section ratio of ^{12}C to ^{9}Be, ^{10}B, and ^{11}B (see Fig. 2, bottom plot). By taking the ratio between solid targets directly, the statistical uncertainty from deuterium is eliminated and the systematic errors are slightly smaller. The slight difference between ^{9}Be (3.2σ) and ^{10}B (1.4σ) is now apparent.

The results shown in Fig. 2 suggest that there is little nuclear dependence of the EMC effect for ^{4}He, ^{9}Be, ^{10}B, ^{11}B, and ^{12}C. While the average of all results for

Target	$\lvert dR_{\mathrm{EMC}}/dx \rvert$	$dR_{^{12}\mathrm{C}/A}/dx$
^{9}Be	0.162 ± 0.024	-0.060 ± 0.019
^{10}B	0.196 ± 0.025	-0.030 ± 0.021
^{11}B	0.217 ± 0.026	-0.010 ± 0.021
^{12}C	0.225 ± 0.024	–

TABLE I. Slopes of EMC ratios extracted in this work. The second column shows the slopes from the A/D ratios while the last column gives the ratios of ^{12}C$/A$ to more precisely study the relative EMC effect in ^{9}Be, ^{10}B, ^{11}B, and ^{12}C.

carbon yields a larger EMC effect than the other nuclei, the average would be significantly smaller if the CLAS data were excluded. In Ref. [4] it was suggested that the relatively large EMC effect in ^{9}Be could be explained by its α cluster structure and the idea that the EMC effect is driven by local density. ^{10}B and ^{11}B are also thought to have significant α cluster contributions to their nuclear structure [23, 24], so the similarity to ^{4}He, ^{9}Be, and ^{12}C serves as confirmation of this hypothesis. Additional data taking for this experiment [13] will also add first measurements of the EMC effect for ^{6}Li and ^{7}Li which will complement the data presented here as the cluster structure in lithium isotopes is also expected to include significant contributions from α clusters, but may differ from the heavier nuclei shown here which have two α clusters.

In summary, we have made the first measurement of the EMC effect in ^{10}B and ^{11}B, providing new information on the nuclear dependence of the EMC effect. The size of the EMC effect for the boron isotopes is similar to that for ^{4}He, ^{9}Be, and ^{12}C, reinforcing the hypothesis that the EMC effect is driven by local, rather than average nuclear density. It will be particularly interesting to see if SRC ratios from the boron isotopes follow the same trend as the EMC effect.

This material is based upon work supported by the U.S. Department of Energy, Office of Science, Office of Nuclear Physics under contracts DE-AC05-06OR23177, DE-AC02-05CH11231, and DE-SC0013615.

[1] J. J. Aubert *et al.* (European Muon), Phys. Lett. B **123**, 275 (1983).
[2] S. Malace, D. Gaskell, D. W. Higinbotham, and I. Cloet, Int. J. Mod. Phys. E **23**, 1430013 (2014).
[3] I. C. Cloët *et al.*, J. Phys. G **46**, 093001 (2019).
[4] J. Seely *et al.*, Phys. Rev. Lett. **103**, 202301 (2009).
[5] N. Fomin *et al.*, Phys. Rev. Lett. **108**, 092502 (2012).
[6] O. Hen, E. Piasetzky, and L. B. Weinstein, Phys. Rev. C **85**, 047301 (2012).
[7] J. Arrington *et al.*, Phys. Rev. C **86**, 065204 (2012).
[8] B. Schmookler *et al.*, Nature **566**, 354 (2019).
[9] J. Arrington and N. Fomin, Phys. Rev. Lett. **123**, 042501 (2019).

[10] J. Arrington, D. Higinbotham, G. Rosner, and M. Sargsian, Prog. Part. Nucl. Phys. **67**, 898 (2012).

[11] N. Fomin, D. Higinbotham, M. Sargsian, and P. Solvignon, Ann. Rev. Nucl. Part. Sci. **67**, 129 (2017).

[12] J. Arrington, N. Fomin, and A. Schmidt, arXiv:2203.02608 (2022), 10.1146/annurev-nucl-102020-022253.

[13] J. Arrington, A. Daniel, N. Fomin, and D. Gaskell, spokespersons, Jefferson lab experiment E12-10-008 (2010).

[14] J. Arrington, D. Day, N. Fomin, and P. Solvignon, spokespersons, Jefferson lab experiment E12-06-105 (2006).

[15] J. Arrington *et al.*, Phys. Rev. C **104**, 065203 (2021).

[16] J. Gomez *et al.*, Phys. Rev. D **49**, 4348 (1994).

[17] L. W. Mo and Y. S. Tsai, Rev. Mod. Phys. **41**, 205 (1969).

[18] Y. S. Tsai, (1971), SLAC-PUB-848.

[19] S. Dasu, P. deBarbaro, A. Bodek, H. Harada, M. Krasny, *et al.*, Phys. Rev. D **49**, 5641 (1994).

[20] J. Arrington, J. G. Rubin, and W. Melnitchouk, Phys. Rev. Lett. **108**, 252001 (2012).

[21] A. Aste, C. von Arx, and D. Trautmann, Eur. Phys. J. **A 26**, 167 (2005).

[22] S. C. Pieper and R. B. Wiringa, Ann. Rev. Nucl. Part. Sci. **51**, 53 (2001).

[23] M. A. Zhusupov, K. A. Zhaksybekova, and R. S. Kabatayeva, Bull. Russ. Acad. Sci. Phys. **84**, 1175 (2020).

[24] N. Itagaki, T. Naito, and Y. Hirata, Phys. Rev. C **105**, 024304 (2022).